

# Orbital Hall effect in transition metals from first-principles scattering calculations

Max Rang and Paul J. Kelly

*Faculty of Science and Technology and MESA<sup>+</sup> Institute for Nanotechnology,  
University of Twente, P.O. Box 217, 7500 AE Enschede, The Netherlands*

(Dated: October 1, 2024)

We use first-principles scattering calculations based upon wave-function matching and implemented with a tight-binding MTO basis to evaluate the orbital Hall conductivity  $\sigma_{\text{oH}}$  for Ti, V, Cr, Cu and Pt metals with temperature-induced lattice disorder. Only interatomic fluxes of orbital angular momentum are included in these estimates; intraatomic fluxes which do not contribute to the transfer of angular momentum are explicitly excluded. The resistivity and orbital Hall angle are both found to be linear in temperature so  $\sigma_{\text{oH}}$  is at most weakly temperature dependent. The value of  $\sigma_{\text{oH}}$  we obtain for bulk Cr is  $\approx 2 \times 10^3 (\hbar/e) (\Omega \text{ cm})^{-1}$  which is substantially lower than previously obtained theoretical results but agrees well with experiment. In units of  $10^3 (\hbar/e) (\Omega \text{ cm})^{-1}$ , the values obtained for Ti, V and Pt are 5, 6 and 7, respectively.

## I. INTRODUCTION

The orbital Hall effect (OHE) [1–3], that is the orbital equivalent of the spin Hall effect (SHE) [4–8], has recently attracted a lot of attention as a source of a current of angular momentum. It is considered to be more fundamental than the SHE [9] and predicted to be significantly larger in size, in particular in systems with weak spin-orbit coupling (SOC) [10, 11]. Its magnitude is typically estimated using a Kubo-like expression for the orbital angular momentum (OAM) conductivity that is analogous to that used to determine the conventional charge conductivity; the similarity of this expression to that for the anomalous Hall effect (AHE) has led to it being called the “orbital Berry curvature” [12, 13]. Computation of the orbital Hall conductivity (OHC) then involves the integration of correlation functions between the OAM current operator  $\mathbf{j}_l$  with elements  $j_{l\gamma}^\beta = \frac{1}{2} \{v_\beta, l_\gamma\}$  and the current operator  $\mathbf{v}$  with elements  $v_\alpha$  where  $\{A, B\}$  is the anticommutator and  $\alpha, \beta, \gamma \in \{x, y, z\}$  [14]; a driving current of charge in the  $\alpha$  direction induces a current of OAM in the  $\beta$  direction that is polarized in the orthogonal  $\gamma$  direction.

In a basis of Wannier functions  $\phi_R$  centred on  $\mathbf{R}$ , the angular momentum can be decomposed into a conventional “intra-atomic” term  $\langle \phi_R | (\mathbf{r} - \mathbf{R}) \times \mathbf{v} | \phi_R \rangle$  and an additional “extra-atomic” term  $\mathbf{R} \times \langle \phi_R | \mathbf{v} | \phi_R \rangle$  that has been shown to be comparable in magnitude to the intra-atomic term in spite of  $\langle \phi_R | \mathbf{v} | \phi_R \rangle$  vanishing for bulk Wannier functions [15]. In calculations of the OHE, this term is more often than not neglected [2, 3, 11, 16] although in the Kubo formalism for infinite “bulk” systems, it has been found to be substantial for materials like gapped graphene [13], MoS<sub>2</sub> bilayers [17] and in the narrow bandgap semiconductors SnTe and PbTe as well as the transition metals V and Pt [18].

Currents are conventionally understood as the flux of some property through a volume and the meaning of the current of a property like  $\mathbf{R} \times \langle \phi_R | \mathbf{v} | \phi_R \rangle$  is unclear. Indeed, to define a current one must define some volume, which necessarily localizes the corresponding property to

that volume. Our intuitive understanding of the OHE, as of the AHE and SHE, involves electrons hopping interatomically, obtaining an anomalous velocity (owing to the Berry curvature). This current is perpendicular to the charge current in general but, depending on the crystal symmetry, can be in any direction [19, 20].

The Kubo expression that is conventionally [10, 11] employed to calculate the “ $X$ ” conductivity tensor, where  $X$  is charge ( $c$ ), spin angular momentum ( $s$ ) or OAM ( $l$ ), is

$$\sigma_{\alpha\beta}^{X\gamma} = \frac{e}{\hbar} \sum_n \int \frac{d^3\mathbf{k}}{(2\pi)^3} f_{n\mathbf{k}} \Omega_{n,\alpha\beta}^{X\gamma}(\mathbf{k}), \quad (1)$$

where

$$\Omega_{n,\alpha\beta}^{X\gamma}(\mathbf{k}) = 2\hbar^2 \sum_{m \neq n} \text{Im} \left[ \frac{\langle u_{n\mathbf{k}} | j_{X\gamma}^\beta | u_{m\mathbf{k}} \rangle \langle u_{m\mathbf{k}} | v_\alpha | u_{n\mathbf{k}} \rangle}{(\varepsilon_{n\mathbf{k}} - \varepsilon_{m\mathbf{k}})^2} \right]. \quad (2)$$

$f_{n\mathbf{k}}$  is the Fermi-Dirac distribution,  $|u_{n\mathbf{k}}\rangle$  is the cell-periodic part of the Bloch state with energy eigenvalue  $\varepsilon_{n\mathbf{k}}$  and the velocity operator is the  $\mathbf{k}$ -derivative of the Hamiltonian

$$v_{\mathbf{k}} = \frac{1}{\hbar} \frac{\partial H_{\mathbf{k}}}{\partial \mathbf{k}} \quad (3)$$

in the crystal momentum representation [21]. Though conceptually simple, this  $\mathbf{k}$ -space formulation of the velocity is beset with mathematical nuance [22] and care must be taken in evaluating (1) and (2) numerically, requiring a very fine discretization of the reciprocal space combined with Wannier interpolation onto the corresponding dense mesh [23, 24]. Performing the calculations in the primitive unit cell of the periodic crystal precludes the direct simulation of disorder.

In this work, we address the orbital Hall conductivity from the point of view of scattering calculations. First, rather than defining the OAM current operator as the orbital analogue of the conventional spin current operator, we begin with a continuity equation for the OAM density on each atom and define the current as the flux

of OAM between atoms. Experimentally, one is interested in the transfer of OAM from some source layer of nonmagnetic material into an adjacent layer of ferromagnetic material. For this to be measurable, it must happen on a length scale that is at least as large as the interatomic distance. By deriving the OAM current from an interatomic flux, we satisfy this requirement theoretically. The precise mathematical relation between the Kubo formula and the method we propose here poses an interesting theoretical challenge, especially as it pertains to currents of spin and orbital angular momenta, but is beyond the scope of the present paper. We will see that the OAM current operator we derive is closely related to the definition of the spin current operator advocated by Niu *et al.* [25] that is still however the topic of discussion [26].

Second, the contribution of atomic disorder, be it chemical (e.g. impurities) or structural (arising from thermal disorder, stacking faults, vacancies, self-interstitials etc.) is not addressed in standard Kubo formula approaches [9–11, 17, 18, 27–29]. Such disorder is present in all samples used in real experiments and its role in determining the OHC needs to be understood. To address this second issue, we will perform quantum mechanical scattering calculations using a wave-function matching (WFM) method [30] implemented [31–33] in a basis of tight-binding (TB) muffin tin orbitals (MTO) [34]. This method allows us to decompose spin and charge currents in terms of the bond currents between atoms. Indeed, in the scattering formalism, only the  $\mathbf{v}_{\text{inter}}$  term contributes to long-range transport. The Twente Quantum Transport (TQT) code [35] has been extended to allow the computation of orbital currents. The relatively low computational cost of running these calculations allows for the treatment of large supercells so that disorder can be treated in real space [36]. In practice, the upper limit for the system size is so large that realistic interfaces, bilayers and thin films can be studied [37–42]. The formalism of bond currents in the atomic spheres approximation allows us to use the conventional OAM operator while still appropriately treating the current on an interatomic footing. To wit, the definition of the velocity operator in the scattering calculations is

$$v = \frac{1}{i\hbar} [\mathbf{r}, H], \quad (4)$$

avoiding problems associated with the  $\mathbf{k}$ -space definition of the velocity [22].

## II. METHOD

A brief overview of the TQT code [35] used in this study is given in Sec. II A. The extension of the WFM formalism implemented in TQT to calculate currents of OAM is presented in Sec. II B. The treatment of disorder as well as additional computational details are described in Sec. II C.

### A. Wave function matching

The geometry is split into three regions, a left lead, a right lead and a scattering region. Left and right leads that are infinitely long in the  $-z$  and  $z$  directions, respectively, sandwich the scattering region in the middle. The time-independent Schrödinger equation is solved for the scattering region with the open boundary conditions corresponding to semi-infinite leads represented by a “self-energy”  $\hat{\Sigma}$ , an energy-dependent potential in the lead layers next to the scattering region. The set of equations to be solved are the system of linear equations

$$(\varepsilon \hat{I} - \hat{H} - \hat{\Sigma}) \Psi = \hat{Q}, \quad (5)$$

where  $\varepsilon$  is the energy of the incoming wave (usually the Fermi energy),  $\hat{H}$  is the Hamiltonian of the scattering region,  $\hat{\Sigma}$  is the self-energy of the coupling with the lead states,  $\Psi$  is the wave function and  $\hat{Q}$  is a source term. The latter are incoming Bloch states, either from the left lead or from the right lead. In the  $z$  direction, the geometry is infinitely long (or finitely long, but with open boundary conditions, according to one’s taste). In the  $x$  and  $y$  directions, we use periodic boundary conditions and “lateral” supercells to simulate disordered materials. In practice, when modelling thermal disorder [36], we find that transport properties scarcely change when the supercell size is increased systematically in the  $x$  and  $y$  directions even when the supercells are as small as  $5 \times 5$  [32, 33]. Further mathematical and computational details of the method can be found in Refs [32, 43].

### B. Orbital currents

Starting with the continuity equation, we derive an expression for the flux of OAM between atoms and discuss the limitations of the approach. Since the wave function is expanded in a localized orbital (TB-MTO) basis, we can write

$$|\Psi\rangle = \sum_P \hat{P} |\Psi\rangle = \sum_P |\Psi_P\rangle, \quad (6)$$

where  $P$  runs over the atoms in the scattering region [33, 38]. In the atomic spheres approximation (ASA), the basis functions centered on different sites  $P$  and  $Q$  are (almost) orthogonal, i.e.,  $\langle \Psi_P | \Psi_Q \rangle \approx \delta_{PQ}$  [44] and we can decompose any local observable as

$$\langle \Psi | \hat{A} | \Psi \rangle = \sum_P \langle \Psi_P | \hat{A} | \Psi_P \rangle. \quad (7)$$

Assuming that  $\hat{\ell}$  is local, i.e.,  $\langle \Psi_P | \hat{\ell} | \Psi_Q \rangle \propto \delta_{PQ}$ , allows us to compute the time derivative of the expectation value of the OAM. Use of the continuity equation relates

this to the flux of OAM out of or into atom  $P$

$$\begin{aligned} \frac{d}{dt} \langle \Psi_P | \hat{\ell} | \Psi_P \rangle &= \left\langle \frac{d\Psi_P}{dt} \left| \hat{\ell} | \Psi_P \rangle + \langle \Psi_P | \hat{\ell} \left| \frac{d\Psi_P}{dt} \right. \right\rangle \\ &= \frac{1}{i\hbar} \left[ \langle \Psi_P | \hat{\ell} \hat{H} | \Psi \rangle - \langle \Psi | \hat{H} \hat{\ell} | \Psi_P \rangle \right] \quad (8) \\ &= \sum_Q j_{\hat{\ell}}^{PQ}. \end{aligned}$$

This equation is completely analogous to a derivation of spin currents in the WFM TB-MTO method and more details can be found in Ref. [33]. The interatomic flux of OAM polarized in the  $\alpha$  direction can be written

$$j_{\hat{\ell}_\alpha}^{PQ} = \frac{1}{i\hbar} \left[ \langle \Psi_P | \hat{\ell}_\alpha \hat{H}_{PQ} | \Psi_Q \rangle - \langle \Psi_Q | \hat{H}_{QP} \hat{\ell}_\alpha | \Psi_P \rangle \right], \quad (9)$$

and, like the spin, the orbital angular momentum is not a conserved quantity so  $j_{\hat{\ell}_\alpha}^{PQ} \neq -j_{\hat{\ell}_\alpha}^{QP}$ . To transform the expression (9) from a flux into a current, it needs to be multiplied by  $\mathbf{d}_{PQ} = \mathbf{r}_P - \mathbf{r}_Q$ , where  $\mathbf{r}_i$  is the position of atom  $i$ . Then, the current of OAM between  $P$  and  $Q$  is

$$\begin{aligned} \bar{j}_{\hat{\ell}_\alpha}^{PQ} &= \frac{1}{2} (\mathbf{r}_P - \mathbf{r}_Q) j_{\hat{\ell}_\alpha}^{PQ} + \frac{1}{2} (\mathbf{r}_Q - \mathbf{r}_P) j_{\hat{\ell}_\alpha}^{QP} \\ &= \frac{\mathbf{r}_P - \mathbf{r}_Q}{2i\hbar} \left[ \langle \Psi_P | \hat{\ell}_\alpha \hat{H}_{PQ} + \hat{H}_{PQ} \hat{\ell}_\alpha | \Psi_Q \rangle \right. \\ &\quad \left. - \langle \Psi_Q | \hat{\ell}_\alpha \hat{H}_{QP} + \hat{H}_{QP} \hat{\ell}_\alpha | \Psi_P \rangle \right]. \quad (10) \end{aligned}$$

This is the expression that is used to obtain the results presented in Sec. III (if the atoms  $P$  and  $Q$  are in the same cell that the orbital current is being averaged over; if they are in different cells, the expression becomes slightly more involved [33]). In practice, we use (9) to calculate interatomic currents which are then processed by analogy with their spin-current-density tensor counterparts  $\vec{j}_s$  to calculate orbital-current-density tensors  $\vec{j}_\ell$  that are either layer-averaged,  $\vec{j}_\ell(z)$  [33], or fully spatially resolved,  $\vec{j}_\ell(\mathbf{r})$  [38].

### C. Disorder and some computational details

When implemented with a minimal basis of localized TB-MTOs [34], the wave-function matching formalism [30] results in a highly sparse system of linear equations [31, 32] that we solve using the MUMPS package [45–47]. The highly efficient sparse solver makes it possible to routinely handle scattering regions containing  $10^4 - 10^5$  atoms but these cannot be distributed arbitrarily in each dimension because of how the memory requirements scale with the lateral supercell size in the  $x$  and  $y$  directions. This constraint is related to the boundary condition imposed by the Bloch nature of the lead states in the “embedding layer”, the last lead layer at the interface between a lead and the scattering region. In a localized orbital representation, the Hamiltonian of the scattering region is highly diagonal. However, the Bloch eigenstates

of the leads have a finite amplitude for these localized orbitals on all atoms of the embedding layer so that the Hamiltonian becomes dense; matrix operations involving the embedding layer ultimately limit the size of problems that can be addressed. As a result, the limit of the lateral supercell size we can currently treat is roughly  $20 \times 20$  for close-packed systems like Pt with a minimal *spd* orbital basis when spin-orbit coupling is included. Still, this supercell is sufficiently large to allow us to construct realistic geometries for systems of current experimental interest like Pt thin films [39, 48].

We model thermal lattice disorder by randomly displacing atoms from their equilibrium positions according to a Gaussian distribution. The variance of this Gaussian is chosen to reproduce the experimental resistivity at a particular temperature [33, 49]. This random disorder is generated for a set of configurations over which transport properties are averaged whereby the number of configurations needed to obtain acceptably converged results is usually 5-10.

Determination of transport properties requires summing over all propagating states at the Fermi energy in the leads. This requires sampling the two-dimensional (2D) Brillouin zone (BZ) corresponding to the in-plane translational symmetry of the scattering region. In practice, we sample the 2D BZ uniformly and experience has shown that a  $160 \times 160$  grid produces very well converged results [31–33]. When a lateral supercell is used, the BZ is folded down so that multiple  $\mathbf{k}$ -points of the original  $1 \times 1$  unit cell can be mapped onto a single  $\mathbf{k}$ -point, which means that to obtain the same accuracy, fewer  $\mathbf{k}$ -points are needed [31]. From now on, we will specify the  $1 \times 1$  equivalent number of  $\mathbf{k}$ -points. For example, a  $160 \times 160$  sampling of the first Brillouin zone (BZ) for a  $1 \times 1$  real space system is equivalent to a  $16 \times 16$  sampling of the BZ for a  $10 \times 10$  lateral supercell. The numbers will not always be nice and round because we always include the  $\Gamma$  point and the number of  $\mathbf{k}$ -points is hence odd. To gain additional insight, we have performed calculations where the Fermi energy is varied and the transport calculation is repeated for the same configuration multiple times, each time at a different energy. All results presented in the following section were obtained using  $7 \times 7$  lateral supercells.

## III. RESULTS

We proceed to calculate the orbital Hall conductivity (OHC) and spin Hall conductivity (SHC) for a number of selected transition metals. In spite of their weak spin-orbit interaction, there is a lot of interest in the  $3d$  transition metals bcc Cr and V that are reported to exhibit large orbital Hall angles [10, 50] as well as for the prototypical and much-used spin Hall material, fcc Pt [8, 51, 52]. To obtain Kohn-Sham ASA potentials for bulk materials, DFT calculations are performed for perfect crystals using the QUESTAAL code [53]. Specif-

ically, the von Barth-Hedin exchange-correlation functional was used [54], with spin-orbit coupling included self-consistently because of the importance of determining the Fermi energy accurately [33]. A minimal *spd* basis of TB-MTOs was used since the transport calculations will be performed using that same basis. As a convergence check, an *spdf* basis was additionally used for Cr. The self-consistent DFT calculations were performed on an  $18 \times 18 \times 18$  **k**-point grid.

The orbital Hall effect can be characterized quantitatively in two different ways. The orbital Hall angle is the ratio of the perpendicular orbital Hall current to the driving charge current which becomes dimensionless when currents of charge and angular momentum are expressed as particle currents [14]. Alternatively, one can compute the orbital Hall conductivity, expressed in units of  $\hbar/e (\Omega \text{ cm})^{-1}$ . The linear response transport formalism we use lends itself naturally to the former since all response currents are expressed per unit driving current. However, in order to directly compare to literature results, we report conductivities here.

Resistivities can be determined by calculating the length dependence of the configuration-averaged resistance [32, 33, 49] requiring calculations for of order five different lengths. Alternatively, one can compute the chemical potential as a function of the position in the scattering region in the direction of transport and obtain the resistivity from a single configuration [55]. The key idea is to determine the slope of the chemical potential within the scattering region by fitting. We can compute the orbital Hall conductivity at some band filling by dividing the average orbital Hall angle within the scattering region by the resistivity computed at that band filling,  $\sigma_{\text{oH}} = \Theta_{\text{oH}}/\rho$ , using the fact that the resistivity  $\rho$  is the inverse of the (charge) conductivity  $\sigma_c$  and using the definition of the orbital Hall angle  $\Theta_{\text{oH}} = j_{\text{oH}}/j_c = \sigma_{\text{oH}}E/\sigma_cE$ , where  $E$  is the electric field.

## A. bcc Cr

### 1. Band filling

The dependence of the spin-Hall and orbital-Hall conductivities calculated for a single configuration of disorder is shown in Fig. 1 as a function of the energy in a rigid band approximation. At the Fermi energy  $\varepsilon_F$ , the value of  $\sigma_{\text{oH}}$  is  $\approx 2 \times 10^3 (\hbar/e) (\Omega \text{ cm})^{-1}$ ; the small SOC for *3d* metals leads to a value of  $\sigma_{\text{sH}}$  that is so small it is virtually indistinguishable from the noise inherent to the single-shot transport calculation, i.e.  $\sim 10 (\hbar/e) (\Omega \text{ cm})^{-1}$ . Taking a different realisation of disorder with the same variance changes  $\sigma_{\text{oH}}(\varepsilon)$  only slightly. In fact, taking a smaller value for the variance of the displacements, corresponding to a lower temperature, only alters the orbital Hall conductivities obtained this way slightly. The low and high temperatures for which the OHC is shown in Fig. 2 correspond to resistivities

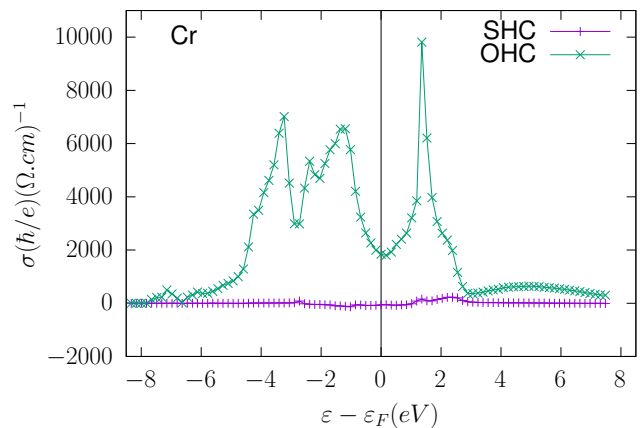


FIG. 1. Energy dependence of the orbital- and spin-Hall conductivities for bulk Cr with thermal lattice disorder corresponding to  $T = 300$  K. The displacements are drawn from a random distribution with a mean square displacement of  $\Delta = 0.085 \text{ \AA}$ .

$\rho \approx 2 \mu\Omega \text{ cm}$  and  $\rho \approx 11 \mu\Omega \text{ cm}$ , respectively. We will see in the next paragraph that the OHC only depends weakly on the mean square displacement  $\Delta^2$  that characterizes the thermal disorder in the scattering region and is proportional to the temperature in the equipartition regime [56]. Because the OHC is roughly constant in  $T$  while the resistivity is linear, the orbital Hall angles for the low and high temperature systems are related to each other as  $\Theta_{\text{oH}} = \rho \sigma_{\text{oH}} \sim T$ , consistent with previous results for the SHA of Pt [57]. The value of the OHC we obtain here is about a factor two lower than other theoretical estimates [10, 11], but agrees rather well with experimental results [50]. Its Fermi energy positions Cr in a deep minimum in  $\sigma_{\text{oH}}$  calculated as a function of en-

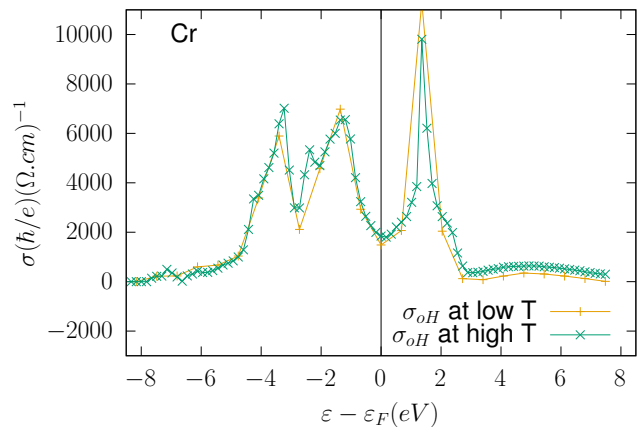


FIG. 2. Energy dependence of the orbital Hall conductivity for Cr for two different values of the rms displacements used to generate thermal lattice disorder. Two different variances are chosen for the displacements of the atoms leading to a “high temperature” and a “low temperature” geometry. These values are  $\Delta_{\text{high}} = 0.085 \text{ \AA}$  and  $\Delta_{\text{low}} = 0.032 \text{ \AA}$ .

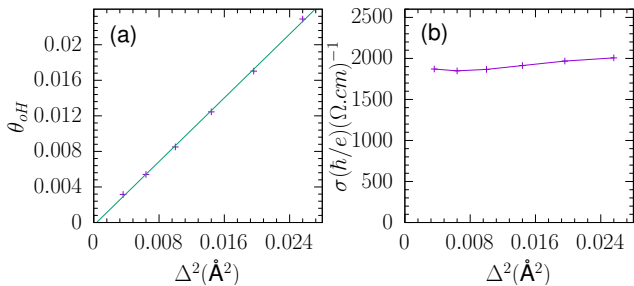


FIG. 3. The orbital Hall angle (a) and the orbital Hall conductivity (b) in Cr as a function of the the mean-square displacement  $\Delta^2$  used to model disorder in the scattering region. The mean square displacement is a proxy for temperature.

ergy (or band-filling). Below we will see that the form of  $\sigma_{\text{oH}}(\varepsilon)$  calculated using the scattering formalism tracks the density of states  $D(\varepsilon)$  closely and the characteristic minimum occurs for all materials we have studied that have the bcc structure. This is in contrast to calculations performed using the Kubo formalism which do not exhibit this minimum in a range of 1 eV around the Fermi energy [10, 11].

## 2. Temperature

By generating geometries for various values of the root mean square displacement, we can simulate the effect of thermal lattice disorder on the orbital Hall effect. The mechanism generating the currents is intrinsic in the sense that there are no crystal defects or impurities. The results shown in Fig. 3(a) show the clear linear dependence of the orbital Hall angle on the mean square displacement of the Cr atoms, which is a proxy for temperature. Because the resistivity is also linear in the mean square displacements, the orbital Hall conductivity is only weakly dependent on temperature as shown in Fig. 3(b) [58].

## B. bcc V

The energy dependence of the OHC for bcc V, shown in Fig. 4, is almost identical to that for Cr which is unsurprising because the materials have the same bcc structure and differ by a single electron. The larger lattice constant of V does not lead to a narrowing of the  $3d$  band because the  $3d$  orbitals are higher in energy and less localized but otherwise, in a rigid band [59] or canonical band [34, 60] approximation, this is the only difference. One electron less in V lowers the Fermi energy and positions it further up a rapidly increasing  $\sigma_{\text{oH}}(\varepsilon)$ . This leads to a substantial increase in the OHC of V at its Fermi energy, with  $\sigma_{\text{oH}} \approx 6 \times 10^3 (\hbar/e) (\Omega \text{ cm})^{-1}$ . The “canonical” form of  $\sigma_{\text{oH}}(\varepsilon)$  for a given crystal structure shows that the value of the OHC can be very sensitive to the band filling. In

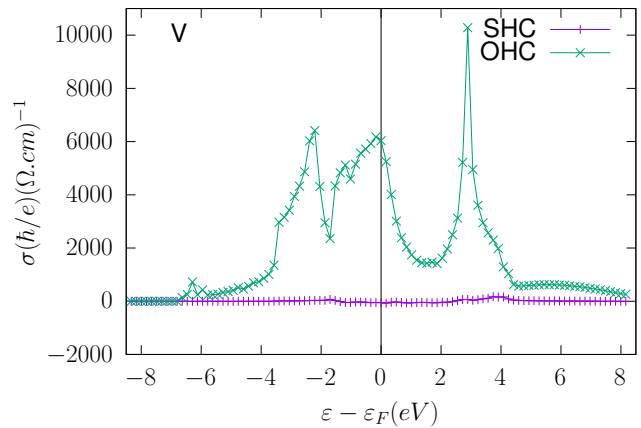


FIG. 4. Fermi energy dependence of the orbital (spin) Hall conductivity for bulk V at room temperature. The rms displacement of the atoms from their equilibrium position is  $\Delta = 0.095 \text{ \AA}$ , corresponding to a resistivity of  $\rho = 20.2 \mu\Omega \text{ cm}$ .

the case of V, shifting the Fermi level up by one eV can result in a reduction of the OHC by a factor three. Fig. 5 shows that there is a strong correlation between the OHC and the density of states, a consequence of final state effects in the scattering formalism [49]. The value we obtain for the OHC at the Fermi level is comparable to the results reported in other computational studies [10, 11] though the band filling dependence is quite different as already mentioned above.

## C. fcc Pt

Our results for the SHC and OHC of Pt are shown in Fig. 6. As a function of the band filling, the SHC agrees reasonably well with previous results [10, 11, 33, 52], with a clear peak at the Fermi level and another, negative, peak centered about 4.5 eV below the Fermi energy both

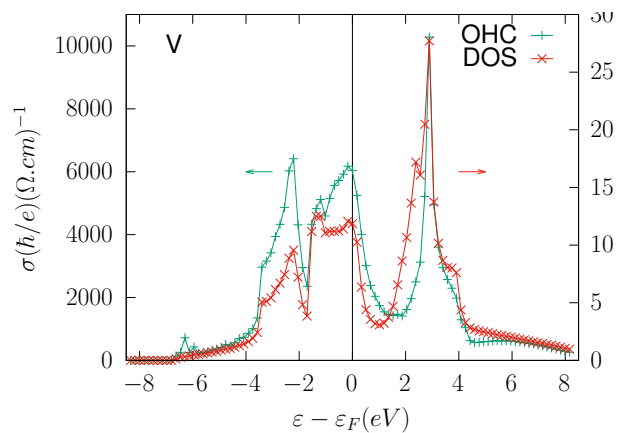


FIG. 5. Energy dependence of (left-hand axis) the orbital Hall conductivity (OHC) for bulk V together with (right-hand axis) the density of states (DOS),  $D(\varepsilon)$ .

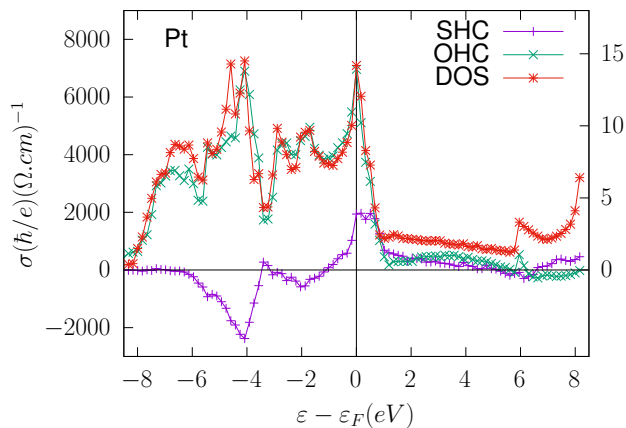


FIG. 6. Fermi energy dependence of (left-hand axis) the orbital (spin) Hall conductivity for bulk Pt at room temperature, meaning the atoms are randomly displaced from equilibrium by a Gaussian distribution with root mean square value  $\Delta = 0.067\text{\AA}$ . The DOS is shown with respect to the right-hand axis.

of which will be slightly reduced when electronic temperature is introduced in the form of the the Fermi-Dirac distribution. These peak structures can be related to the SOC-induced splitting of orbitally degenerate states at points and along lines of high symmetry [52]. In spite of including thermal lattice broadening, we consistently find more structure in both  $\sigma_{sH}(\varepsilon)$  and  $\sigma_{oH}(\varepsilon)$  with our scattering calculations than found using the Kubo formalism. Part of this discrepancy may come from the huge value of lifetime broadening (0.4 eV) used by Salemi and Oppeneer [11] which, while perhaps appropriate for optical experiments, is less obviously justified for transport measurements where the lifetime diverges at the Fermi energy in the absence of disorder; no explanation is given for the failure of  $\sigma_{oH}(\varepsilon)$  to vanish for energies below the bottom of the conduction bands. The reason for the lack of structure in the  $\sigma_{oH}(\varepsilon)$  calculated by Jo *et al.* is not clear.

Focussing on the value of the OHC at the Fermi level, our scattering calculations predict a larger value of  $\sigma_{oH}(\varepsilon_F) \approx 7 \times 10^3 (\hbar/e)(\Omega \text{cm})^{-1}$  than the Kubo calculations. This large OHC value might partially explain the large variance in experimental values of the SHA in Pt (see Table V in [33]). For example, in a Pt|FM bilayer geometry of Pt adjacent to a ferromagnet (FM), an orbital current generated in the Pt layer is injected simultaneously with a spin current, where the orbital-to-spin conversion at the interface and in the FM layer determines the magnitude of the resulting orbital torque [61–63]. We expect that the interface conversion of orbital to spin current will depend on details of the interface atomic structure; this should be taken into account in the analysis of spin-orbit torque experiments in any case.

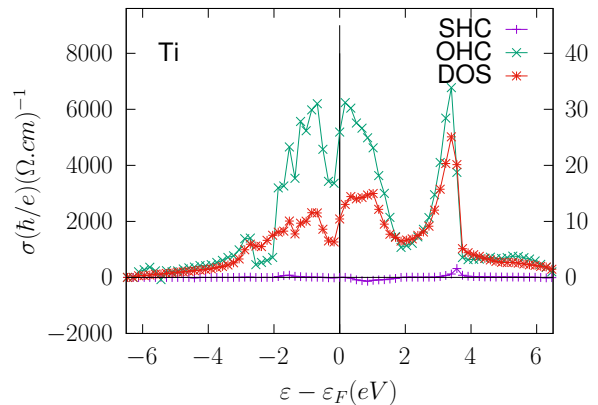


FIG. 7. Fermi energy dependence of the orbital Hall conductivity for bulk Ti at finite temperature, meaning the atoms are randomly displaced from equilibrium by a Gaussian distribution with root mean square value  $\Delta = 0.085\text{\AA}$  ( $0.095\text{\AA}$ ), corresponding to a bulk resistivity of  $\rho = 32 \mu\Omega \cdot \text{cm}$  ( $40.5 \mu\Omega \cdot \text{cm}$ ).

#### D. hcp Ti

Having performed calculations for transition metal systems with bcc and fcc crystal structures, we complete the set of elementary crystal structures by calculating the OHC for hcp Ti. For Cr we explicitly showed that the OHC was independent of temperature. We now avoid the (expensive) iterative determination of the rms displacements corresponding to room temperature resistivity for Ti by assuming that the OHC is independent of temperature. We model thermal lattice disorder with values of  $\Delta = 0.085\text{\AA}$  ( $0.095\text{\AA}$ ), which correspond to bulk resistivities of  $\rho = 32 \mu\Omega \text{cm}$  ( $40.5 \mu\Omega \text{cm}$ ). These are lower than the room temperature resistivity of  $\rho = 48.6 \mu\Omega \text{cm}$  [64]. The band filling dependence of the OHC is shown in Fig. 7 and we find (not shown) that its temperature dependence is marginal, once again illustrating the insensitivity to thermal disorder. The OHC parallels the structure in the DOS as a function of energy but to a lesser extent than for the bcc and fcc structures. The OHC at the Fermi level is  $\sigma_{oH} \approx 5 \times 10^3 (\hbar/e)(\Omega \text{cm})^{-1}$ .

#### E. fcc Cu

Repeating the procedure for fcc Cu yields more interesting results, Fig. 8. In particular, we see large values of the SHC in the energy region between 1 and 4 eV below the Fermi energy. This contradicts the received wisdom that the SOC in  $3d$  elements is too weak to yield significant spin Hall conductivities, failing to take into consideration the much smaller bandwidth of  $3d$  bands. The OHC we find at the Fermi level is  $\sigma_{oH}(\varepsilon_F) \approx 200 (\hbar/e)(\Omega \text{cm})^{-1}$ , much smaller than values of  $\sim 1 \times 10^3 (\hbar/e)(\Omega \text{cm})^{-1}$  found using the Kubo for-

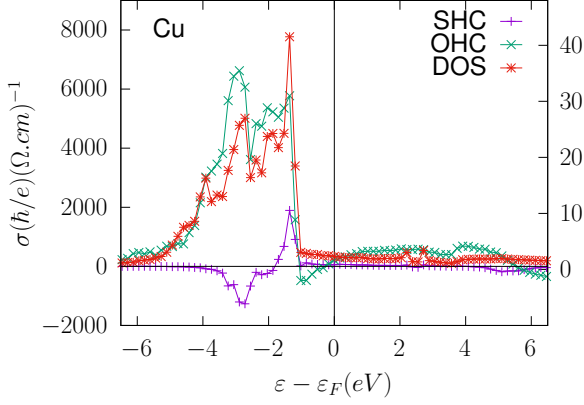


FIG. 8. Fermi energy dependence of the orbital Hall conductivity for bulk Cu at temperature, meaning the atoms are randomly displaced from equilibrium by a Gaussian distribution with root mean square value  $\Delta = 0.08\text{\AA}$ .

mula [10, 11]. More recent computational work addressing some of the mathematical problems encountered by the  $\mathbf{k}$ -space definition of the velocity has even predicted a negative value of  $\sigma_{\text{OH}}(\varepsilon_F) = -1 \times 10^3 (\hbar/e)(\Omega \text{ cm})^{-1}$  [24].

#### IV. DISCUSSION

We have calculated the orbital Hall conductivity for Ti, V, Cr, Cu and Pt with the same first-principles scattering theory used to determine the relaxation length of currents of non-equilibrium OAM injected from orbitally polarized leads into thermally disordered “bulk” materials [65]. The expression for the orbital current in terms of flux is inherently interatomic, in contrast to the conventional Kubo-formula expression. In this context, the conventional intra-atomic OAM operator we used (in the so-called atom-centered approximation) is reasonable es-

pecially when using the atomic spheres approximation where all of space is filled with atomic spheres and the volume of the interstitial region is implicitly set to zero; this is in contrast to FLAPW calculations where a substantial interstitial region is neglected [11].

The orbital Hall conductivity calculated here for Cr agrees well with values extracted from experiment [50] and in the case of Pt agrees reasonably well with previous calculations [10, 11]. We attribute differences between values of the OHC obtained with scattering theory and the Kubo formalism to the exclusion of purely intra-atomic currents in the former. We propose that such currents cannot contribute to the interatomic flux of orbital angular momentum. Such contributions are difficult to exclude from the Kubo formula though a direct comparison might yield interesting insights. It is peculiar that in the case of the SHC of Pt, there is almost no difference between results obtained with the Kubo and scattering formalisms.

Finally, we have shown that the OHC is robust against thermal disorder. Like the SHC, the OHC seems to be more or less independent of temperature corresponding to a linear dependence on temperature of the orbital Hall angle.

##### A. Alternative definition of orbital angular momentum current

In this section, we want to connect with other theoretical work. This typically starts with a definition of the orbital current operator whereas we arrived at an expression for a current of OAM between two atoms  $P$  and  $Q$  in Sec. II B by applying the continuity equation to the expectation value of  $\hat{\ell}$  assuming it to be local, i.e., without invoking a definition.

Our starting point is the expression (10) for a current of “ $X$ ” between atoms  $P$  and  $Q$  where, as in (1) and (2), “ $X$ ” is charge ( $c$ ), spin angular momentum ( $s$ ) or OAM ( $l$ ). The first term of (10),  $(\mathbf{r}_P - \mathbf{r}_Q) j_X^{PQ}$

$$\begin{aligned} (\mathbf{r}_P - \mathbf{r}_Q) j_X^{PQ} &= \frac{\mathbf{r}_P - \mathbf{r}_Q}{i\hbar} \left[ \langle \Psi_P | \hat{X} \hat{H}_{PQ} | \Psi_Q \rangle - \langle \Psi_Q | \hat{H}_{QP} \hat{X} | \Psi_P \rangle \right] \\ &= \frac{1}{i\hbar} \left[ \langle \Psi_P | \mathbf{r}_P \hat{X} \hat{H}_{PQ} - \hat{X} \hat{H}_{PQ} \mathbf{r}_Q | \Psi_Q \rangle + \langle \Psi_Q | \mathbf{r}_Q \hat{H}_{QP} \hat{X} - \hat{H}_{QP} \hat{X} \mathbf{r}_P | \Psi_P \rangle \right] \end{aligned} \quad (11)$$

can be simplified using the localization of the MTO basis to write  $\mathbf{r}_P | \Psi_P \rangle \approx \hat{r} | \Psi_P \rangle$ . Because the basis functions are not eigenstates of the position operator, the intra-atomic position (also called the “fractional” part [66]) is lost in this approximation. As stated in the introduction, we propose that these intra-atomic currents do not actually contribute to the spin or orbital Hall currents. Then

$$(\mathbf{r}_P - \mathbf{r}_Q) j_X^{PQ} = \frac{1}{i\hbar} \left[ \langle \Psi_P | \hat{r} \hat{X} \hat{H} - \hat{X} \hat{H} \hat{r} | \Psi_Q \rangle + \langle \Psi_Q | \hat{r} \hat{H} \hat{X} - \hat{H} \hat{X} \hat{r} | \Psi_P \rangle \right] \quad (12a)$$

$$= \frac{1}{i\hbar} \left[ \langle \Psi_P | [\hat{r}, \hat{X} \hat{H}] | \Psi_Q \rangle + \langle \Psi_Q | [\hat{r}, \hat{H} \hat{X}] | \Psi_P \rangle \right]. \quad (12b)$$

### 1. Charge

For a charge current ( $X = c$ ),  $\hat{X} = -e\hat{I}$ , where  $-e$  is the electron charge and  $\hat{I}$  is the identity operator. The expression for the charge current becomes

$$(\mathbf{r}_P - \mathbf{r}_Q) j_c^{PQ} = -\frac{e}{i\hbar} \left[ \langle \Psi_P | [\hat{r}, \hat{H}] | \Psi_Q \rangle + \langle \Psi_Q | [\hat{r}, \hat{H}] | \Psi_P \rangle \right] = \langle \Psi_P | \hat{j}_c | \Psi_Q \rangle + \langle \Psi_Q | \hat{j}_c | \Psi_P \rangle \quad (13)$$

where we have used the definition of the velocity and current operators

$$\hat{j}_c = -e\hat{v} = -\frac{e}{i\hbar} [\hat{r}, \hat{H}]. \quad (14)$$

Since charge conservation requires that  $j_c^{PQ} = -j_c^{QP}$ , the final expression for  $\bar{j}_c^{PQ}$  remains

$$\bar{j}_c^{PQ} = \langle \Psi_P | \hat{j}_c | \Psi_Q \rangle + \langle \Psi_Q | \hat{j}_c | \Psi_P \rangle \quad (15)$$

and the description of interatomic electron currents in the transport formulation used here is consistent with the usual definition of the current operator used in the Kubo formalism.

### 2. Spin

For spin, ( $X = s$ ),  $\hat{X} = \hat{s}_\alpha = \frac{\hbar}{2}\sigma_\alpha$ , where  $\sigma_\alpha$  are the Pauli matrices and  $\alpha \in \{x, y, z\}$ , the spin current between  $P$  and  $Q$  becomes

$$\begin{aligned} (\mathbf{r}_P - \mathbf{r}_Q) j_{s\alpha}^{PQ} \\ = \frac{1}{i\hbar} \left[ \langle \Psi_P | [\hat{r}, \hat{s}_\alpha \hat{H}] | \Psi_Q \rangle + \langle \Psi_Q | [\hat{r}, \hat{H} \hat{s}_\alpha] | \Psi_P \rangle \right], \end{aligned} \quad (16)$$

and similarly the spin current between  $Q$  and  $P$  is

$$\begin{aligned} (\mathbf{r}_Q - \mathbf{r}_P) j_{s\alpha}^{QP} \\ = \frac{1}{i\hbar} \left[ \langle \Psi_Q | [\hat{r}, \hat{s}_\alpha \hat{H}] | \Psi_P \rangle + \langle \Psi_P | [\hat{r}, \hat{H} \hat{s}_\alpha] | \Psi_Q \rangle \right], \end{aligned} \quad (17)$$

suggesting the definition of a spin current operator of

$$\begin{aligned} \hat{j}_{s\alpha} &= \frac{1}{2i\hbar} \left( [\hat{r}, \hat{s}_\alpha \hat{H}] + [\hat{r}, \hat{H} \hat{s}_\alpha] \right) \\ &= \frac{1}{2i\hbar} \left( \hat{r} \hat{s}_\alpha \hat{H} - \hat{s}_\alpha \hat{H} \hat{r} + \hat{r} \hat{H} \hat{s}_\alpha - \hat{H} \hat{s}_\alpha \hat{r} \right). \end{aligned} \quad (18)$$

This expression is similar, but not identical, to the conventional spin current operator

$$\begin{aligned} \hat{j}_{s\alpha}^{\text{conv}} &= \frac{1}{2i\hbar} \left( \hat{s}_\alpha [\hat{r}, \hat{H}] + [\hat{r}, \hat{H}] \hat{s}_\alpha \right) \\ &= \frac{1}{2i\hbar} \left( \hat{s}_\alpha \hat{r} \hat{H} - \hat{s}_\alpha \hat{H} \hat{r} + \hat{r} \hat{H} \hat{s}_\alpha - \hat{H} \hat{r} \hat{s}_\alpha \right). \end{aligned} \quad (19)$$

The definitions coincide exactly when  $[\hat{r}, \hat{s}_\alpha] = 0$ , i.e. when the position and spin operators commute. This assumption is automatically satisfied in the approximation

that the intra-atomic position operator is very small compared to the inter-atomic position, i.e.  $\hat{r} |\Psi_P\rangle \approx \mathbf{r}_P |\Psi_P\rangle$ . In conclusion, in the scattering formalism, the spin current operator that can be derived from the continuity equation is exactly equivalent to the conventional definition of the spin current operator used elsewhere, notably in the Kubo formalism.

We should mention that there is not yet a consensus about the correct form of the spin current operator. A mostly mathematically motivated case exists for the so-called ‘‘proper’’ spin current operator [25, 26], defined as

$$\hat{j}_{s\alpha}^{\text{prop}} = \frac{1}{i\hbar} [\hat{r} \hat{s}_\alpha, \hat{H}] = \frac{1}{i\hbar} \left( \hat{r} \hat{s}_\alpha \hat{H} - \hat{H} \hat{r} \hat{s}_\alpha \right), \quad (20)$$

which is only equal to the other two definitions described above when  $[\hat{H}, \hat{s}_\alpha] = 0$ , i.e., in the absence of SOC. Although this ‘‘proper’’ definition has been described as being more accurate than the conventional description, we are not aware of any first-principles calculations of spin Hall conductivities that use it.

### 3. Orbital Angular Momentum

For orbital currents ( $X = l$ ), the operator becomes  $\hat{X} = \hat{l}_\alpha$ , with  $x \in \{x, y, z\}$  and the derivation is identical to the spin current case, yielding the orbital current operator

$$\begin{aligned} \hat{j}_{l\alpha} &= \frac{1}{2i\hbar} \left( [\hat{r}, \hat{l}_\alpha \hat{H}] + [\hat{r}, \hat{H} \hat{l}_\alpha] \right) \\ &= \frac{1}{2i\hbar} \left( \hat{r} \hat{l}_\alpha \hat{H} - \hat{l}_\alpha \hat{H} \hat{r} + \hat{r} \hat{H} \hat{l}_\alpha - \hat{H} \hat{l}_\alpha \hat{r} \right), \end{aligned} \quad (21)$$

that is (as in the spin case) similar to, but not identical to, the conventional orbital current operator

$$\begin{aligned} \hat{j}_{l\alpha}^{\text{conv}} &= \frac{1}{2i\hbar} \left( \hat{l}_\alpha [\hat{r}, \hat{H}] + [\hat{r}, \hat{H}] \hat{l}_\alpha \right) \\ &= \frac{1}{2i\hbar} \left( \hat{l}_\alpha \hat{r} \hat{H} - \hat{l}_\alpha \hat{H} \hat{r} + \hat{r} \hat{H} \hat{l}_\alpha - \hat{H} \hat{r} \hat{l}_\alpha \right). \end{aligned} \quad (22)$$

Again, the expressions are equivalent when  $[\hat{r}, \hat{l}_\alpha] = 0$ . In this picture, the commutation of  $\hat{r}$  and  $\hat{l}$  is mathematically expressed by the approximation of the position operator  $\hat{r} |\Psi_P\rangle \approx \mathbf{r}_P |\Psi_P\rangle$ , which means that the position operator becomes diagonal in the localized basis, together with the assumption that the matrix element  $\langle \Psi_P | \hat{l}_\alpha | \Psi_Q \rangle$  is zero for  $P \neq Q$ . Only then do  $\hat{r}$  and



$\hat{\ell}$  commute. If  $\langle \Psi_P | \hat{\ell}_\alpha | \Psi_Q \rangle \neq 0$ , it becomes impossible to define the OAM current as a flux from  $P$  to  $Q$ , and the current will instead be absorbed into the torque term in the continuity equation. This is the mathematical equivalent of the statement that it is impossible to define a current of something which is not localized. One can only define the flux of something which can be described in local terms. Mathematically, one might define a flux from atoms  $P$  and  $Q$  together, into another set of atoms  $R$  and  $S$ , but the sheer number of fluxes to possible pairs of atoms rapidly becomes intractable. The method of computing orbital currents presented above is thus limited to systems for which the atomic spheres approximation (ASA) is reasonable, thus excluding materials such as graphene [13] where each atom has only three nearest neighbours and, to a lesser extent, the transition metal dichalcogenides [17] and narrow-gap semiconductors SnTe and PbTe [18] with six nearest neighbours. There should be a clear and unambiguous association of each point in space with a particular atomic center with respect to which the orbital angular momentum can be calculated.

## V. CONCLUSION

Starting from the continuity equation, we expressed the orbital Hall effect in terms of interatomic currents of

intra-atomic orbital moments and calculated  $\sigma_{\text{oH}}(\varepsilon)$  for bcc Cr, bcc V, fcc Pt, hcp Ti and fcc Cu, all at or close to room temperature. Though the magnitude of the OHC is comparable to values calculated using the Kubo formalism by others [10, 11], the band filling dependence  $\sigma_{\text{oH}}(n) \equiv \sigma_{\text{oH}}(n(\varepsilon))$  is found to be quite different resulting in an orbital Hall conductivity that is substantially lower for Cr, comparable for Ti, V and Cu and substantially larger for Pt.  $\sigma_{\text{oH}}(\varepsilon)$  has much more structure and correlates strongly with the density of states. The orbital Hall conductivity, like the spin Hall conductivity, is insensitive to changes in temperature, corresponding to linear scaling of both Hall angles and resistivity with temperature. That the angular momentum current due to the orbital Hall effect is not suppressed by thermal disorder is welcome news for technological applications.

## ACKNOWLEDGEMENTS

This work was sponsored by NWO Domain Science for the use of supercomputer facilities.

- 
- [1] B. A. Bernevig, T. L. Hughes, and S.-C. Zhang, Orbitoronics: The intrinsic orbital current in p-doped silicon, *Phys. Rev. Lett.* **95**, 066601 (2005).
- [2] T. Tanaka, H. Kontani, M. Naito, T. Naito, D. S. Hirashima, K. Yamada, and J. Inoue, Intrinsic spin Hall effect and orbital Hall effect in  $4d$  and  $5d$  transition metals, *Phys. Rev. B* **77**, 165117 (2008).
- [3] H. Kontani, T. Tanaka, D. S. Hirashima, K. Yamada, and J. Inoue, Giant Orbital Hall Effect in Transition Metals: Origin of Large Spin and Anomalous Hall Effects, *Phys. Rev. Lett.* **102**, 016601 (2009).
- [4] M. I. D'yakonov and V. I. Perel, Possibility of orienting electron spins with current, *Zh. Eksp. Teor. Fiz.* **13**, 657 (1971), [*JETP Letters-USSR* 13, pp 467-469 (1971)].
- [5] M. I. Dyakonov and V. I. Perel, Current-induced spin orientation of electrons in semiconductors, *Phys. Lett. A* **35**, 459 (1971).
- [6] J. E. Hirsch, Spin Hall Effect, *Phys. Rev. Lett.* **83**, 1834 (1999).
- [7] A. Hoffmann, Spin Hall effects in metals, *IEEE Trans. Magn.* **49**, 5172 (2013).
- [8] J. Sinova, S. O. Valenzuela, J. Wunderlich, C. H. Back, and T. Jungwirth, Spin Hall effects, *Rev. Mod. Phys.* **87**, 1213 (2015).
- [9] D. Go, D. Jo, C. Kim, and H.-W. Lee, Intrinsic Spin and Orbital Hall Effects from Orbital Texture, *Phys. Rev. Lett.* **121**, 086602 (2018).
- [10] D. Jo, D. Go, and H.-W. Lee, Gigantic intrinsic orbital hall effects in weakly spin-orbit coupled metals, *Phys. Rev. B* **98**, 214405 (2018).
- [11] L. Salemi and P. M. Oppeneer, First-principles theory of intrinsic spin and orbital Hall and Nernst effects in metallic monoatomic crystals, *Phys. Rev. Materials* **6**, 095001 (2022).
- [12] I. Baek and H.-W. Lee, Negative intrinsic orbital Hall effect in group XIV materials, *Phys. Rev. B* **104**, 245204 (2021).
- [13] S. Bhowal and G. Vignale, Orbital Hall effect as an alternative to valley Hall effect in gapped graphene, *Phys. Rev. B* **103**, 195309 (2021).
- [14] For convenience, we measure the charge density in units of the electron charge  $-e$  (where  $e$  is a positive quantity), the spin density in units of  $\hbar/2$  and the orbital density in units of  $\hbar$  so they all become particle densities and the fluxes become particle fluxes.
- [15] T. Thonhauser, D. Ceresoli, D. Vanderbilt, and R. Resta, Orbital Magnetization in Periodic Insulators, *Phys. Rev. Lett.* **95**, 137205 (2005).
- [16] D. Go, F. Freimuth, J.-P. Hanke, F. Xue, O. Gomonay, K.-J. Lee, S. Blügel, P. M. Haney, H.-W. Lee, and Y. Mokrousov, Theory of current-induced angular momentum transfer dynamics in spin-orbit coupled systems, *Phys. Rev. Research* **2**, 033401 (2020).
- [17] T. P. Cysne, S. Bhowal, G. Vignale, and T. G. Rapoport, Orbital Hall effect in bilayer transition metal dichalcogenides: From the intra-atomic approximation to the Bloch states orbital magnetic moment approach, *Phys. Rev. B* **105**, 195421 (2022).

- [18] A. Pezo, D. G. Ovalle, and A. Manchon, Orbital Hall effect in crystals: Interatomic versus intra-atomic contributions, *Phys. Rev. B* **106**, 104414 (2022).
- [19] M. Seemann, D. Ködderitzsch, S. Wimmer, and H. Ebert, Symmetry-imposed shape of linear response tensors, *Phys. Rev. B* **92**, 155138 (2015).
- [20] A. Roy, M. H. D. Guimarães, and J. Sławińska, Unconventional spin Hall effects in nonmagnetic solids, *Phys. Rev. Materials* **6**, 045004 (2022).
- [21] J. Callaway, *Quantum Theory of the Solid State* (Academic Press, New York, 1974).
- [22] J. J. Esteve-Paredes and J. J. Palacios, A comprehensive study of the velocity, momentum and position matrix elements for Bloch states: Application to a local orbital basis, *SciPost Phys. Core* **6**, 002 (2023).
- [23] M. Zeer, D. Go, J. P. Carbone, T. G. Saunderson, M. Redies, M. Kläui, J. Ghabboun, W. Wulfhekel, S. Blügel, and Y. Mokrousov, Spin and orbital transport in rare-earth dichalcogenides: The case of  $\text{EuS}_2$ , *Phys. Rev. Materials* **6**, 074004 (2022).
- [24] D. Go, H.-W. Lee, P. M. Oppeneer, S. Blügel, and Y. Mokrousov, First-principles calculation of orbital Hall effect by Wannier interpolation: Role of orbital dependence of the anomalous position, *Phys. Rev. B* **109**, 174435 (2024).
- [25] J. Shi, P. Zhang, D. Xiao, and Q. Niu, Proper Definition of Spin Current in Spin-Orbit Coupled Systems, *Phys. Rev. Lett.* **96**, 076604 (2006); P. Zhang, Z. Wang, J. Shi, D. Xiao, and Q. Niu, Theory of conserved spin current and its application to a two-dimensional hole gas, *Phys. Rev. B* **77**, 075304 (2008).
- [26] G. Marcelli, G. Panati, and S. Teufel, A New Approach to Transport Coefficients in the Quantum Spin Hall Effect, *Annales Henri Poincaré* **22**, 1069 (2021).
- [27] T. P. Cysne, M. Costa, L. M. Canonico, M. B. Nardelli, R. B. Muniz, and T. G. Rappoport, Disentangling Orbital and Valley Hall Effects in Bilayers of Transition Metal Dichalcogenides, *Phys. Rev. Lett.* **126**, 056601 (2021).
- [28] S. Bhowal and S. Satpathy, Intrinsic orbital moment and prediction of a large orbital Hall effect in two-dimensional transition metal dichalcogenides, *Phys. Rev. B* **101**, 121112(R) (2020).
- [29] S. Bhowal and S. Satpathy, Intrinsic orbital and spin Hall effects in monolayer transition metal dichalcogenides, *Phys. Rev. B* **102**, 035409 (2020).
- [30] T. Ando, Quantum point contacts in magnetic fields, *Phys. Rev. B* **44**, 8017 (1991).
- [31] K. Xia, M. Zwierzycki, M. Talanana, P. J. Kelly, and G. E. W. Bauer, First-principles scattering matrices for spin-transport, *Phys. Rev. B* **73**, 064420 (2006).
- [32] A. A. Starikov, Y. Liu, Z. Yuan, and P. J. Kelly, Calculating the transport properties of magnetic materials from first-principles including thermal and alloy disorder, non-collinearity and spin-orbit coupling, *Phys. Rev. B* **97**, 214415 (2018).
- [33] R. J. H. Wesselink, K. Gupta, Z. Yuan, and P. J. Kelly, Calculating spin transport properties from first principles: spin currents, *Phys. Rev. B* **99**, 144409 (2019).
- [34] O. K. Andersen and O. Jepsen, Explicit, First-Principles Tight-Binding Theory, *Phys. Rev. Lett.* **53**, 2571 (1984); O. K. Andersen, O. Jepsen, and D. Glözel, Canonical description of the band structures of metals, in *Proceedings of the International School of Physics ‘Enrico Fermi’* (Consorzio IXXI, P. Hohenberg, Ed., North-Holland, Amsterdam, 1983) pp. 1–17, available from <https://www2.fkf.mpg.de/andersen/docs/pub/abstract/and1985-6.html>; O. K. Andersen, Z. Pawłowska, and O. Jepsen, Illustration of the linear-muffin-tin-orbital tight-binding representation: Compact orbitals and charge density in Si, *Phys. Rev. B* **34**, 5253 (1986).
- [35] <https://github.com/MaxRang/TwenteQuantumTransport>.
- [36] Y. Liu, A. A. Starikov, Z. Yuan, and P. J. Kelly, First-principles calculations of magnetization relaxation in pure Fe, Co, and Ni with frozen thermal lattice disorder, *Phys. Rev. B* **84**, 014412 (2011); Y. Liu, Z. Yuan, R. J. H. Wesselink, A. A. Starikov, M. van Schilfgaarde, and P. J. Kelly, Direct method for calculating temperature-dependent transport properties, *Phys. Rev. B* **91**, 220405(R) (2015).
- [37] K. Gupta, R. J. H. Wesselink, R. Liu, Z. Yuan, and P. J. Kelly, Disorder Dependence of Interface Spin Memory Loss, *Phys. Rev. Lett.* **124**, 087702 (2020).
- [38] R. S. Nair and P. J. Kelly, Fully resolved currents from quantum transport calculations, *Phys. Rev. B* **103**, 195406 (2021).
- [39] R. S. Nair, M. S. Rang, and P. J. Kelly, Spin Hall Effect in a Thin Pt Film, *Phys. Rev. B* **104**, L220411 (2021).
- [40] K. Gupta, R. J. H. Wesselink, Z. Yuan, and P. J. Kelly, Spin transport at finite temperatures: A first-principles study for ferromagnetic|nonmagnetic interfaces, *Phys. Rev. B* **104**, 205426 (2021).
- [41] R. Liu, K. Gupta, Z. Yuan, and P. J. Kelly, Calculating the spin memory loss at Cu|metal interfaces from first principles, *Phys. Rev. B* **106**, 014401 (2022).
- [42] K. Gupta, R. Liu, R. J. H. Wesselink, Z. Yuan, and P. J. Kelly, Calculating interface transport parameters at finite temperatures: Nonmagnetic interfaces, *Phys. Rev. B* **106**, 115425 (2022).
- [43] P. A. Khomyakov, G. Brocks, V. Karpan, M. Zwierzycki, and P. J. Kelly, Conductance calculations for quantum wires and interfaces: mode matching and Green functions, *Phys. Rev. B* **72**, 035450 (2005).
- [44] Assuming that  $\varepsilon = \varepsilon_\nu = \varepsilon_F$  and neglecting three-center terms.
- [45] P. R. Amestoy, I. S. Duff, and J. Y. L’Excellent, Multifrontal parallel distributed symmetric and unsymmetric solvers, *Comput. Methods Appl. Mech. Eng.* **184**, 501 (2000).
- [46] P. R. Amestoy, I. S. Duff, J. Koster, and J. Y. L’Excellent, A fully asynchronous multifrontal solver using distributed dynamic scheduling, *SIAM J. Matrix Anal. Appl.* **23**, 15 (2001).
- [47] P. R. Amestoy, A. Guermouche, J. Y. L’Excellent, and S. Pralet, Hybrid scheduling for the parallel solution of linear systems, *Parallel Computing* **32**, 136 (2006).
- [48] C. Stamm, C. Murer, M. Berritta, J. Feng, M. Gabureac, P. M. Oppeneer, and P. Gambardella, Magneto-Optical Detection of the Spin Hall Effect in Pt and W Thin Films, *Phys. Rev. Lett.* **119**, 087203 (2017).
- [49] R. S. Nair, E. Barati, K. Gupta, Z. Yuan, and P. J. Kelly, Spin-Flip Diffusion Length in  $5d$  Transition Metal Elements: a First-Principles Benchmark, *Phys. Rev. Lett.* **126**, 196601 (2021).
- [50] G. Sala and P. Gambardella, Giant orbital Hall effect and orbital-to-spin conversion in  $3d$ ,  $5d$ , and  $4f$  metallic heterostructures, *Phys. Rev. Lett.* **123**, 087203 (2022).

- [51] T. Kimura, Y. Otani, T. Sato, S. Takahashi, and S. Maekawa, Room-Temperature Reversible Spin Hall Effect, *Phys. Rev. Lett.* **98**, 156601 (2007).
- [52] G. Y. Guo, S. Murakami, T.-W. Chen, and N. Nagaosa, Intrinsic Spin Hall Effect in Platinum: First-Principles Calculations, *Phys. Rev. Lett.* **100**, 096401 (2008).
- [53] D. Pashov, S. Acharya, W. R. Lambrecht, J. Jackson, K. D. Belashchenko, A. Chantis, F. Jamet, and M. van Schilfgaarde, Questaal: A package of electronic structure methods based on the linear muffin-tin orbital technique, *Comput. Phys. Commun.* **249**, 107065 (2020).
- [54] U. von Barth and L. Hedin, A local exchange-correlation potential for the spin-polarized case: I, *J. Phys. C: Sol. State Phys.* **5**, 1629 (1972).
- [55] R. J. H. Wesselink, Y. Liu, Z. Yuan, A. A. Starikov, A. N. Other, S. W. Els, and P. J. Kelly, unpublished (2014).
- [56] Though the onset of the equipartition regime is strictly speaking at the Debye temperature  $\Theta_D$ , “in practice the high- $T$  limit is identified as the equipartition regime with linear-in- $T$  resistivity ... but can extend practically to about  $T > \Theta_D/3$  in Pt, Cu and Au and to about  $T > \Theta_D/5$  in Al” [58]. For typical transition-metal Debye temperatures, this means for  $T > 100$  K [49].
- [57] L. Wang, R. J. H. Wesselink, Y. Liu, Z. Yuan, K. Xia, and P. J. Kelly, Giant Room Temperature Interface Spin Hall and Inverse Spin Hall Effects, *Phys. Rev. Lett.* **116**, 196602 (2016).
- [58] C. Xiao, Y. Liu, Z. Yuan, S. A. Yang, and Q. Niu, Temperature dependence of the side-jump spin Hall conductivity, *Phys. Rev. B* **100**, 085425 (2019).
- [59] J. Kübler, *Theory of Itinerant Electron Magnetism* (Oxford University Press, Oxford, 2000).
- [60] A. R. Mackintosh and O. K. Andersen, The electronic structure of transition metals, in *Electrons at the Fermi Surface*, edited by M. Springford (Cambridge University Press, Cambridge, 1980) pp. 149–224.
- [61] D. Go and H.-W. Lee, Orbital torque: Torque generation by orbital current injection, *Phys. Rev. Research* **2**, 013177 (2020).
- [62] S. Lee, M.-G. Fang, D. Go, D. Kim, J.-H. Kang, T. Lee, G.-H. Lee, J. Hang, N. J. Lee, Y. Mokrousov, S. Kim, K.-J. Kim, K.-J. Lee, and B.-G. Park, Efficient conversion of orbital Hall current to spin current for spin-orbit torque switching, *Communications Physics* **4**, 234 (2021).
- [63] D. Lee, D. Go, H.-J. Park, W. Jeong, H.-W. Ko, D. Yun, D. Jo, S. Lee, G. Go, J. H. Oh, K.-J. Kim, B.-C. Min, H. C. Koo, H.-W. Lee, O. Lee, B.-G. Park, and K.-J. Lee, Orbital torque in magnetic bilayers, *Nat. Commun.* **12**, 6710 (2021).
- [64] E. A. Bel’skaya, An Experimental Investigation of the Electrical Resistivity of Titanium in the Temperature Range from 77 to 1600 K, *High Temperature* **43**, 546–553 (2005).
- [65] M. S. Rang and P. J. Kelly, Orbital relaxation length from first-principles scattering calculations, *Phys. Rev. B* **109**, 214427 (2024).
- [66] I. Turek, J. Kudrnovský, V. Drchal, L. Szunyogh, and P. Weinberger, Interatomic electron transport by semiempirical and ab-initio tight-binding approaches, *Phys. Rev. B* **65**, 125101 (2002).